Article ID: 1000-324X(2023)05-0577-06 **DOI:** 10.15541/jim20220318

Heavy-Fermion $YbAl_3$ Materials: One-step Synthesis and Enhanced Thermoelectric Performance

HE Danqi[1], WEI Mingxu[2], LIU Ruizhi[2], TANG Zhixin[2], ZHAI Pengcheng[1], ZHAO Wenyu[3]

(1. Hubei Key Laboratory of Theory and Application of Advanced Materials Mechanics, Wuhan University of Technology, Wuhan 430070, China; 2. International School of Materials Science and Engineering, Wuhan University of Technology, Wuhan 430070, China; 3. State Key Laboratory of Advanced Technology for Materials Synthesis and Processing, Wuhan University of Technology, Wuhan 430070, China)

Abstract: Microstructure plays a key role in tuning physical properties of materials. Here $YbAl_3$ materials with high figure of merit ZT of 0.35 at 300 K was directly synthesized with Yb and Al pure powders through one-step spark plasma sintering process in 10 min. The excellent thermoelectric performance is attributed to the simultaneous reduction in the lattice thermal conductivity by 47% and electronic thermal conductivity by 27% at 300 K. The remarkable decrease in the electronic thermal conductivity is ascribed to the enhanced scattering of electrons by nanocrystals with 5–20 nm in diameter, strip-like non-crystal with several nanometers in width and various atomic-scale distortions. The substantial decline in the lattice thermal conductivity originates from the enhanced scattering of phonons due to multi-scale microstructures spanning from nanoscale to mesoscale. This work demonstrates that one-step spark plasma sintering process is an efficient strategy to rapidly synthesize $YbAl_3$ materials with multi-scale microstructures and enhanced thermoelectric performance.

Key words: $YbAl_3$ thermoelectric materials; one-step synthesis; microstructure; thermoelectric performance

Thermoelectric (TE) materials have attracted increasing attention because of fascinating applications in recycling industrial waste heat, cooling microelectronics and integrated circuits, and generating power using automobile exhaust heat and full-spectrum solar energy[1]. The conversion efficiency of TE materials is determined by the dimensionless figure of merit $ZT=\alpha^2\sigma T/\kappa$, where T, α, σ, and κ are the absolute temperature, Seebeck coefficient, electrical conductivity, and total thermal conductivity ($\kappa=\kappa_E+\kappa_L$, where κ_E is the electronic contribution and κ_L the lattice contribution), respectively. Good thermoelectric material should be the perfect combination of high power factor ($\alpha^2\sigma$) and low thermal conductivity[2]. To improve the thermal transport properties, various phonon engineering approaches have been used to enhance phonon scattering and restrict κ_L[3-5]. To optimize the electric transport properties, a series of band structure engineering approaches have been developed to promote σ, α and/or $\alpha^2\sigma$[6-8]. However, it is extremely hard to simultaneously promote α and σ, meanwhile reduce κ because of the conflicting TE material properties.

$YbAl_3$ TE material has attracted considerable attention due to its potential application in Peltier cooling. As a typical heavy-fermion TE material, $YbAl_3$ has very high σ due to its metallic conducting behavior and considerably large α because of the hybridization of Yb4f electrons with itinerant counterparts[9-10], and $\alpha^2\sigma$ of $YbAl_3$ is about 3 times higher than that of Bi_2Te_3, which is one of the state-of-the-art TE materials. However, ZT of $YbAl_3$ is much lower than that of Bi_2Te_3 because of the high κ rooted from high σ and simple cubic crystal structure of $YbAl_3$[11-24]. Various complicated methods have been developed to synthesize $YbAl_3$ materials, which includes self-flux growth combined with etching and hot-pressing [15,19], arc melting followed by annealing and hot- pressing[12], Bridgman growth combined with etching and hot-

Received date: 2022-06-05; **Revised date:** 2022-06-27; **Published online:** 2022-07-08
Foundation item: National Key Research and Development Program of China (2018YFB0703603, 2019YFA0704903); National Natural Science Foundation of China (11834012, 52130203, 52102298); Foshan Xianhu Laboratory of the Advanced Energy Scienc eand Technology Guangdong Laboratory (XHT2020-004); National Innovation And Entrepreneurship Training Program for College Students (312040000245)
Biography: HE Danqi (1990–), lecturer. E-mail: hedanqi@whut.edu.cn
贺丹琪(1990–), 讲师. E-mail: hedanqi@whut.edu.cn
Corresponding author: ZHAO Wenyu, professor. E-mail: wyzhao@whut.edu.cn
赵文俞, 教授. E-mail: wyzhao@whut.edu.cn

pressing[11,13], arc melting combined with etching, ball milling, and pulsed electric current sintering[16,21-22], and directly melting followed by annealing and spark plasma sintering (SPS)[12,23-24]. All of these traditional methods not only take long time for the crystallization of $YbAl_3$ compound but also own multi-step processes. Especially, there are only micron- and mesoscale microstructures in $YbAl_3$ materials prepared in literature. These coarse microstructures only scatter phonon and decrease κ_L but have no effect on electrical transport properties. To optimize the electric transport properties of $YbAl_3$, various doping attempts, including doping at the Yb and Al sites and filling the Al_6 octahedral voids with external atoms, have been employed to tailor $\alpha^2\sigma$[17-24]. Unfortunately, these attempts are not effective in suppressing κ and σ, because the major component of high κ is κ_E rather than κ_L. According to the Wiedemann–Franz law ($\kappa_E=L\sigma T$), for $YbAl_3$ decreasing σ seems to be a reasonable option to lower κ_E and κ. Nevertheless, the theoretical and experimental results showed that doping at Yb and Al sites in $YbAl_3$ did not distinctly affect the band structure and thus did not significantly decline σ. Therefore, how to reduce σ of $YbAl_3$ has become an important subject to make a breakthrough in ZT. In this work, a one-step method was developed by SPS process to synthesize single-phase $YbAl_3$ materials. The one-step synthesis not only costs less time but also aims to form multi-scale microstructures that simultaneously scatter electrons and phonons.

1 Experimental

The highly pure Al and Yb powders with nominal composition $YbAl_{3.2}$ were mixed in an agate mortar and then directly sintered for 10 min by SPS process (Dr Sinter, SPS-1050) under the condition of 50 MPa, 873 K and Ar atmosphere. Two samples were labeled as SPS1 and SPS2. For comparison, one sample labeled as MQA-SPS was prepared by a traditional method of melting, quenching, annealing and SPS, which took 7 d[25]. The phase constituents of samples were determined by powder X-ray diffraction (XRD, PANalytical *X'* Pert PRO) using Cu Kα radiation. The microstructures were examined by field emission scanning electron microscope (FESEM, Zeiss ULTRA-PLUS-43-13). High resolution transmission electron microscope (HRTEM) images were observed using a transmission electron microscope (JEOL-2100F). σ and α were measured with the standard four-probe method (Ulvac Riko, ZEM-3) in Ar atmosphere. κ was calculated using the equation $\kappa=C_p\lambda\rho$, where C_p is the specific heat capacity, ρ is the bulk density and λ is the thermal diffusion coefficient. λ was measured by laser flash technique (Netzsch LFA 427) in flowing Ar atmosphere. ρ was measured by Archimedes method. C_p was measued by TA Q20 differential scanning calorimeter (DSC). κ_E was calculated by the Wiedemann-Franz law($\kappa_E=LT\sigma$), where the Lorentz number L has a numerical value of 1.6×10^{-8} $V^2\cdot K^{-2}$ estimated by Rowe *et al*[13]. κ_L was obtained by subtracting κ_E from κ based on the equation $\kappa_L=\kappa-\kappa_E$. Uncertainties are ±7% for σ and κ, and ±5% for α.

2 Results and discussion

Fig. 1 displays XRD patterns of SPS1, SPS2 and MQA-SPS samples. All diffraction peaks can be indexed to $YbAl_3$ (JCPDS 65-0957), indicating that three samples are composed of single-phase $YbAl_3$. The result demonstrates that single-phase $YbAl_3$ materials can be directly synthesized with Yb and Al raw powders through one-step SPS process. FESEM images (Fig. 2) show the obvious difference in microstructures between SPS*n* and MQA-SPS samples on the micron scale. Like the majority of $YbAl_3$ materials prepared by traditional processes, MQA-SPS exhibits mesoscopic-scale microstructures

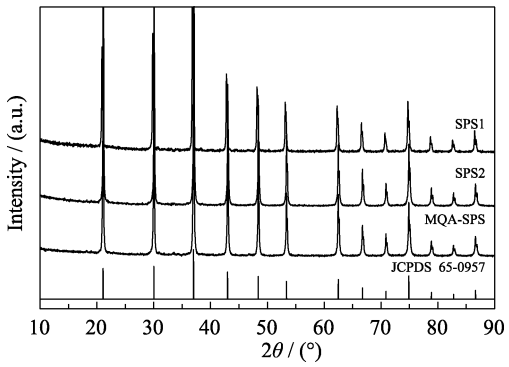

Fig. 1 XRD patterns of SPS1, SPS2 and MQA-SPS samples

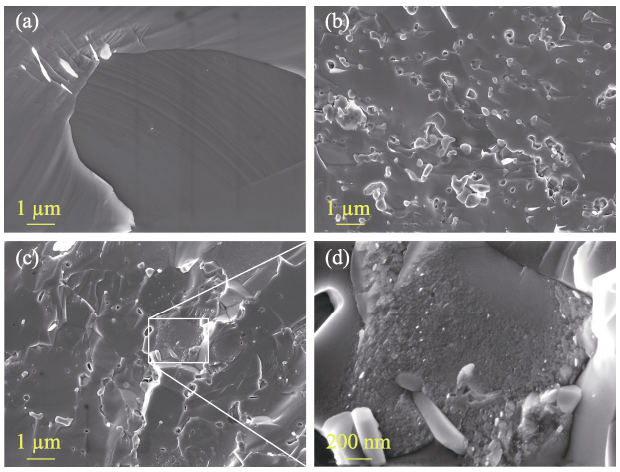

Fig. 2 Microstructures of SPS1, SPS2 and MQA-SPS samples (a-c) FESEM images of (a) MQA-SPS, (b) SPS1, and (c) SPS2; (d) Enlarged FESEM image of the rectangular region in (c)

that are composed of micrometer-sized crystals, as shown in Fig. 2(a). However, besides mesoscopic-scale microstructures, there are a large number of grain boundaries, nanocrystals and nano-pores in SPS*n*, as shown in Fig. 2(b-d).

In order to further characterize various microstructures in SPS*n*, the HRTEM images were investigated. The results were shown in Fig. 3 as exampled by SPS1. The insets are inversed fast Fourier transferred (IFFT) images of the marked regions. It can be seen that SPS*n* are composed of nanocrystals, strip-like noncrystal, and various dislocations. $YbAl_3$ nanocrystals with 5–20 nm in diameter reveal different diffraction contrast as shown in Fig. 3(a), indicating that these nanocrystals have different crystal orientation. The strip-like noncrystal with several nanometers in width occurs in big $YbAl_3$ perfect crystals as shown in Fig. 3(b), being attributed to the synergistic effects of the fast synthesis and pressure. Various atomic-scale defects are induced and accumulated in $YbAl_3$ nanocrystals as shown in Fig. 3(c, d), which are distorted arrays (left inset in Fig. 3(c)), edge dislocations (right inset in Fig. 3(c) and left inset in Fig. 3(d)), faults occurring at distorted layer interfaces (right inset in Fig. 3(d)), and small-angle grain boundaries (marked with yellow lines in Fig. 3(d)). Therefore, these multi-scale microstructures in SPS*n* samples span from the atomic scale, nanometer sizes, to mesoscale.

The temperature dependences of electrical conductivity, Seebeck coefficient for SPS1, SPS2, and MQA-SPS in the temperature range of 300–500 K are shown in Fig. 4. The inset in Fig. 4(b) displays the temperature dependence of power factor. All samples have negative α over the whole temperature range, implying n-type conduction. σ of all samples gradually reduced as temperature increasing in the range of 300–500 K owing to the enhanced scattering of carriers and phonons on crystal lattice[26]. It is worth noting that σ of SPS*n* samples significantly descends as compared to that of MQA-SPS sample, which can be reasonably explained with enhanced electron scattering induced by $YbAl_3$ nanocrystals with 5–20 nm in diameter, nanoscale strip-like noncrystal and various atomic-scale distortions. As shown in Fig. 4(b), the absolute values of α for SPS*n* samples are higher than that of MQA-SPS, which attributes to the decline of σ. The highest α of SPS samples reaches about –85 $\mu V \cdot K^{-1}$ at 300 K which is much higher than that of other intermetallic compounds and close to the data reported by Rowe[11]. Compared with MQA-SPS, σ of SPS*n* samples at 300 K are decreased by 15% and α value of SPS*n* samples at 300 K are increased by 8%. As a result, the $\alpha^2\sigma$ values of two SPS*n* samples are higher than that of MQA-SPS, showing that the electric transport properties of $YbAl_3$ materials prepared by one-step method are better than those of $YbAl_3$ materials synthesized by traditional method.

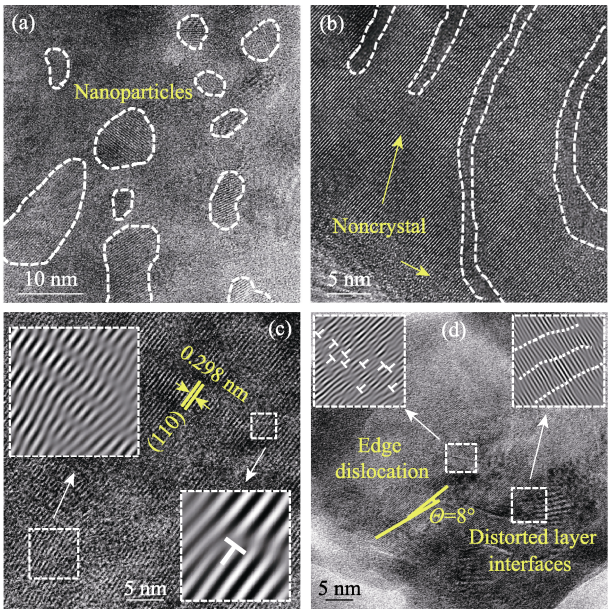

Fig. 3　Multi-scale microstructures in SPS1

(a) HRTEM image of $YbAl_3$ nanocrystals with 5–20 nm in diameter; (b) HRTEM image of nanoscale strip-like noncrystal in $YbAl_3$ crystals; (c, d) HRTEM images of high-density distortions in $YbAl_3$ crystals with insets showing IFFT images of the marked regions

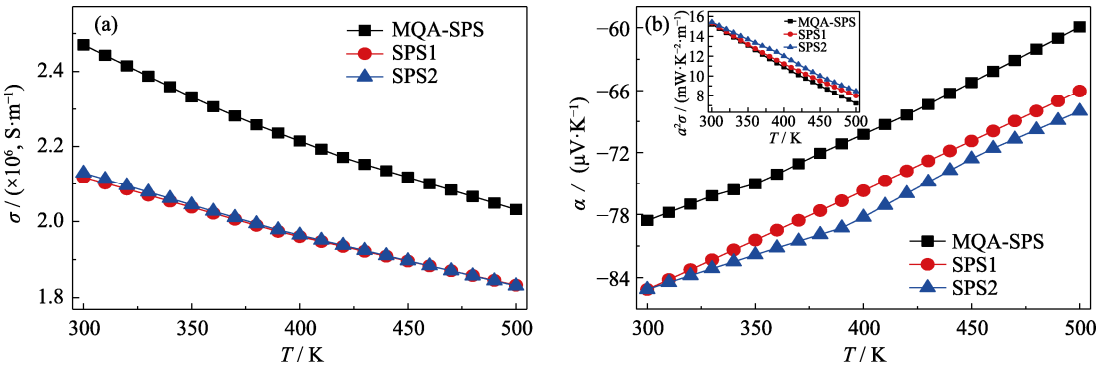

Fig. 4　Temperature dependence of (a) electrical conductivity and (b) Seebeck coefficient for SPS1, SPS2 and MQA-SPS with inset showing the temperature dependence of power factor

These temperature dependences of electrical transport properties undoubtedly reveal that the multi-scale microstructures in the heavy-fermion $YbAl_3$ play beneficial roles in decreasing σ. It is necessary to explain why the multi-scale microstructures are so important for σ of $YbAl_3$ materials. The theoretical studies about the heavy-fermion $YbAl_3$ based on the first-principle calculation and Boltzmann transport theory showed that the nanostructures with less than 30 nm in size could strongly scatter the electrons and cause the substantial decline in σ of $YbAl_3$, the calculated σ and κ_E of $YbAl_3$ effectively decreased at 300 K when the mean free path was less than 30 nm[27]. The theoretical discovery has been confirmed by our previous experimental result[28]. Therefore, the remarkable decline in σ of SPSn samples is firmly ascribed to the nanocrystals with 5–20 nm in diameter, nanoscale strip-like noncrystal and various atomic-scale distortions scattering electrons.

Fig. 5 displays the temperature dependences of (a) thermal conductivity, (b) carrier thermal conductivity, (c) lattice thermal conductivity, and (d) ZT of all samples. κ of all samples ascended with increasing temperature in the range of 300–500 K, exhibiting metallic heat conduction behavior. κ of SPS1 and SPS2 are far less than those of MQA-SPS, indicating that the multi-scale microstructures in SPS1 and SPS2 can significantly reduce κ. As shown in Fig. 5(a, b), κ and κ_E of SPS1 and SPS2 at 300 K significantly fell from 19.7 and 14.8 $W \cdot K^{-1} \cdot m^{-1}$ for MQA-SPS to 13.4 and 10.8 $W \cdot K^{-1} \cdot m^{-1}$, decreased by 32% and 27%, respectively. The significant decline in κ_E values of SPS1 and SPS2 are attributed to the contribution of the reduced σ. Meanwhile, it is worth noting that κ_L values of SPSn samples are much lower than that of MQA-SPS in the range 300–500 K, decreased by 47% at 300 K. The remarkable reduction in κ_L of SPSn samples is attributed to the broad-frequency phonon scattering induced by the multi-scale microstructures (Fig. 3), indicating that κ_L of $YbAl_3$ materials substantially descends through various microstructures rather than doping or filling. The similar phenomenon that κ_L effectively decreased with multi-scale microstructures was reported by some important TE materials such as hierarchical architectures in PbTe[3], micro- and nanopores in $CoSb_3$[4], and multi-scale microstructures in Bi_2Te_3[29]. Therefore, the multi-scale microstructures through one-step SPS method can simultaneously decrease κ_E and κ_L, resulting in lower κ of $YbAl_3$ TE materials.

ZT values were calculated according to the measured α, σ and κ in the range of 300–500 K, and the results were shown in Fig. 5(d). It is worth noting that ZT values of SPS1 and SPS2 are much larger than that of MQA-SPS. The maximum ZT reached 0.35 at 300 K for SPS2, increased by 49% as compared with MQA-SPS. Meanwhile, the maximum ZT outperforms all undoped $YbAl_3$ materials reported by other groups[11,13,20], suggesting that the multi-microstructures from one-step synthesis process can substantially improve the TE properties of $YbAl_3$ materials. The remarkable decline in σ and κ plays a key

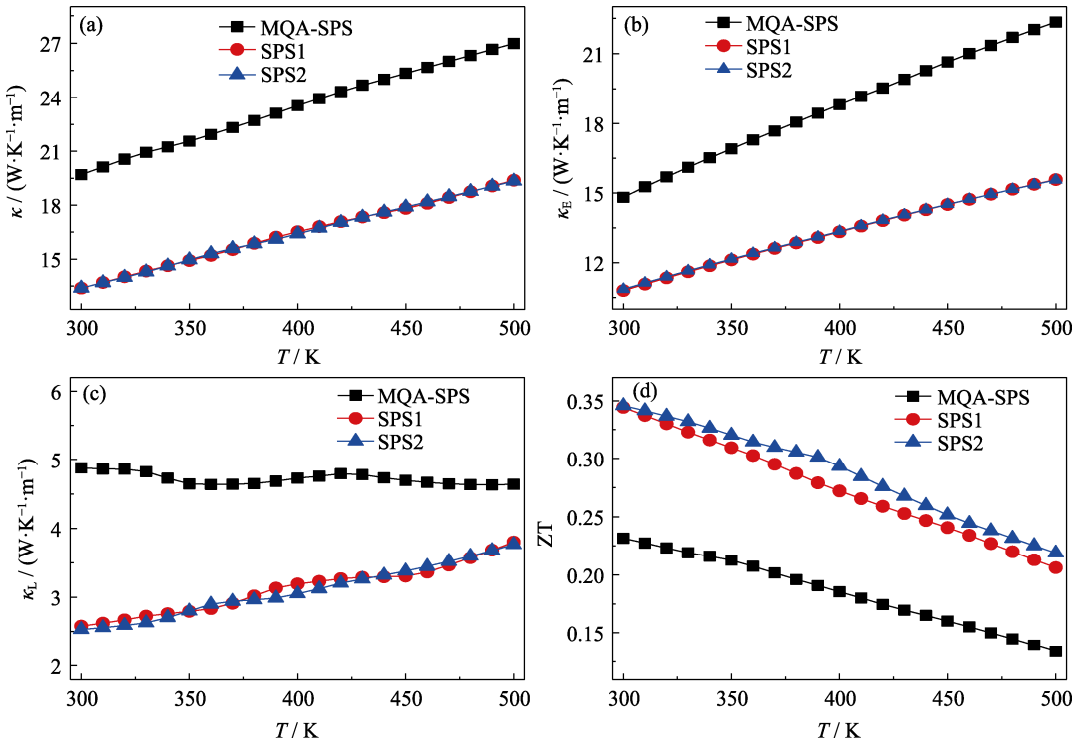

Fig. 5 Temperature dependences of (a) thermal conductivity, (b) carrier thermal conductivity, (c) lattice thermal conductivity, and (d) ZT values for the samples for SPS1, SPS2 and MQA-SPS

role in enhancing ZT values for SPS*n* samples. The decreased σ results in significant rise of α, and the electric property of $YbAl_3$ materials is enhanced through the compromise between σ and α. In addition, the enhanced electron and phonon scattering reduces κ_E and κ_L, respectively. As a result, SPS*n* samples fabricated by one-step SPS process display very low κ.

3 Conclusions

In summary, a one-step SPS method was developed to synthesize $YbAl_3$ materials. The results from XRD, FESEM and HRTEM confirm that single-phase $YbAl_3$ materials with multi-scale microstructures spanning from atomic scale, nanometer sizes, to mesoscale was directly formed in 10 min from Yb and Al elements with this method. It is found that the nanocrystals with 5–20 nm in diameter, nanoscale strip-like noncrystal and various atomic-scale distortions effectively scatter electrons and significantly reduce σ and κ_E, while other hierarchical microstructures spanning from nanometer size to mesoscale can strongly scatter phonons and remarkably decrease κ_L. As a result, σ, κ, κ_L and κ_E at 300 K for SPS*n* samples descended by 15%, 32%, 47% and 27%, as compared with MQA-SPS. Meanwhile, α and ZT ascended by 8% and 49%, respectively. The maximum ZT is about 0.35 at 300 K. This work demonstrated that the multi-scale microstructures obtained through one-step SPS method can simultaneously optimize all TE parameters of heavy-fermion $YbAl_3$ materials.

References:

[1] BELL L E. Cooling, heating, generating power, and recovering waste heat with thermoelectric systems. *Science*, 2008, **321(5895):** 1457.

[2] KIM H S, LIU W S, REN Z F. Bridge between materials and devices of thermoelectric power generators. *Energy Environment Science*, 2017, **10(1):** 69.

[3] BISWAS K, HE J Q, BLUM I D, *et al.* High-performance bulk thermoelectrics with all-scale hierarchical architectures. *Nature*, 2012, **489(7416):** 414.

[4] YU J, ZHAO W Y, WEI P, *et al.* Enhanced thermoelectric performance of (Ba,In) double-filled skutterudites *via* randomly arranged micropores. *Applied Physics Letters*, 2014, **104:** 142104.

[5] XU Z J, WU H J, ZHU T J, *et al.* Attaining high mid-temperature performance in $(Bi,Sb)_2Te_3$ thermoelectric materials *via* synergistic optimization. *NPG Asia Materials*, 2016, **8:** e302.

[6] WU D, ZHAO L D, HAO S Q, *et al.* Origin of the high performance in GeTe-based thermoelectric materials upon Bi_2Te_3 doping. *Journal of the American Chemical Society*, 2014, **136(32):** 11412.

[7] MAO J, KIM H, SHUAI S J, *et al.* Thermoelectric properties of materials near the band crossing line in Mg_2Sn-Mg_2Ge-Mg_2Si system. *Acta Materials*, 2016, **103:** 633.

[8] ZHANG J, SONG L R, PEDERSEN S H, *et al.* Discovery of high-performance low-cost n-type Mg_3Sb_2-based thermoelectric materials with multi-valley conduction bands. *Nature Communications*, 2017, **8:** 13901.

[9] STEWART G R, FISK Z, WIRE M S. New Ce heavy-Fermion system: $CeCu_6$. *Physical Review B*, 1984, **30(1):** 482.

[10] STRANGE P, SVANE A, TEMMERMAN W M, *et al.* Understanding the valency of rare earths from first-principles theory. *Nature*, 1999, **399(6738):** 756.

[11] ROWE D M, MIN G, KUZNESTSOV V L. Thermoelectric properties of not-pressed $YbAl_3$ compound over temperature range 150–800 K. 16th International Conference on Thermoelectrics, Dresden, 1997**:** 528.

[12] ROWE D M, MIN G, KUZNESTSOV V L. Electrical resistivity and Seebeck coefficient of hot-pressed $YbAl_3$ over the temperature range 150–700 K. *Philosophical Magazine Letters,* 1998, **77(2):** 105.

[13] ROWE D M, KUZNETSOV V L, KUZNETSOVA L A, *et al.* Electrical and thermal transport properties of intermediate-valence $YbAl_3$. *Journal of Applied Physics*, 2002, **35(17):** 2183.

[14] HE T, CALVARESE T G, CHEN J Z, *et al.* Origin of low thermal conductivity in α-Mn: enhancing the ZT of $YbAl_3$ and $CoSb_3$ through Mn addition. 24th International Conference on Thermoelectrics, Clemson, 2005**:** 437.

[15] CHRISTIANSON A D, FANELLI V R, LAWRENCE J M, *et al.* Localized excitation in the hybridization gap in $YbAl_3$. *Physical Review Letters*, 2006, **96(11):** 117206.

[16] ROJAS D P, FERNÁNDEZ BARQUÍN L, ESPESO J I, *et al.* Reduction of the Yb valence in $YbAl_3$ nanoparticles. *Physical Review B*, 2008, **78(9):** 094412.

[17] ZHOU J, SUN Z M, CHENG X, *et al.* Phase stability and electronic structures of $YbAl_{3-x}M_x$ (M=Mg, Cu, Zn, In and Sn) studied by first-principles calculations. *Intermetallics*, 2009, **17(12):** 995.

[18] CHEN C K, SANG X H, CUI W J, *et al.* Atomic-resolution fine structure and chemical reaction mechanism of Gd/$YbAl_3$ thermoelectric-magnetocaloric heterointerface. *Journal of Alloys and Compounds*, 2020, **831:** 154722.

[19] OČKO M, ŽONJA S, AVIANI I, *et al.* Transport properties of the $YbAl_3$ compound: on the energy scales of $YbAl_3$ from thermopower data. *Journal of Alloys and Compounds*, 2011, **509:** 6999.

[20] KATSUYAMA S, SUZUKI M, TANAKA T. Effect of addition of B or C on thermoelectric properties of heavy fermion intermetallic compound $YbAl_3$. *Journal of Alloys and Compounds*, 2012, **513:** 189.

[21] LEHR G J, MORELLI D T. Synthesis, crystal structure, and thermoelectric properties of the $YbAl_3$-$ScAl_3$ solid solution. *Intermetallics*, 2013, **32:** 225.

[22] LEHR G J, MORELLI D T. Thermoelectric properties of $Yb_{1-x}(Er,Lu)_xAl_3$ solid solutions. *Journal of Electronic Materials*, 2013, **42(7):** 1697.

[23] LI J Q, LIU X Y, LI Y, *et al.* Influence of Sn substitution on the thermoelectric properties in $YbAl_3$. *Journal of Alloys and Compounds*, 2014, **600:** 8.

[24] LI J Q, LIU X Y, LI Y, *et al.* Effects of second phase Yb_5Sb_3 on the thermoelectric properties of $YbAl_3$. *Journal of Electronic Materials*, 2014, **43(4):** 1289.

[25] HE D Q, ZHAO W Y, MU X, *et al.* Preparation and thermoelectric properties of $YbAl_3$ thermoelectric materials with excessive Al. *Journal of Electronic Materials*, 2015, **44(6):** 1919.

[26] ZHAO W Y, WEI P, ZHANG Q J, *et al.* Enhanced thermoelectric performance in barium and indium double-filled skutterudite bulk materials *via* orbital hybridization induced by Indium filler. *Journal of the American Chemical Society*, 2009, **131(10):** 3713.

[27] LIANG J H, FAN D D, JIANG P H, *et al.* First-principles study of the thermoelectric properties of intermetallic compound $YbAl_3$. *Intermetallics*, 2017, **87:** 27.

[28] HE D Q, ZHAO W Y, MU X, *et al.* Enhanced thermoelectric

performance of heavy-fermion $YbAl_3$ *via* multi-scale microstructures. *Journal of Alloys and Compounds*, 2017, **725:** 1297.
[29] HU L P, GAO H L, LIU X H, *et al.* Enhancement in thermoelectric performance of bismuth telluride based alloys by multi-scale microstructural effects. *Journal of Materials Chemistry*, 2012, **22(32):** 16484.

一步法制备重费米子 $YbAl_3$ 热电材料及其性能提升

贺丹琪[1], 魏明旭[2], 刘蒌之[2], 汤志鑫[2], 翟鹏程[1], 赵文俞[3]

(武汉理工大学 1. 新材料力学理论与应用湖北省重点实验室; 2. 材料科学与工程国际化示范学院; 3. 材料复合新技术国家重点实验室, 武汉 430070)

摘 要: 材料的微观结构对其物理性能调控起着至关重要的作用。本研究以 Yb 和 Al 单质为原料, 采用放电等离子烧结工艺通过一步法快速合成 $YbAl_3$ 材料。显微结构表明, 快速制备的 $YbAl_3$ 材料内部含有大量微米尺度晶粒、纳米晶粒、纳米非晶带和多种原子尺度位错等丰富的多尺度微结构, 这些多尺度微结构可以同时增强 $YbAl_3$ 材料的电子和声子散射, 进而同时降低其晶格热导率(47%)和电子热导率(27%), 使得总热导率降低至 13.4 $W\cdot K^{-1}\cdot m^{-1}$, $YbAl_3$ 材料的最大 ZT 可达 0.35。该研究表明, 通过一步法放电等离子烧结工艺可以快速合成具有多尺度微结构的高热电性能 $YbAl_3$ 块体材料。

关 键 词: $YbAl_3$ 热电材料; 一步法合成; 微结构; 热电性能

中图分类号: TQ174 **文献标志码:** A